

## RESEARCH ARTICLE

# Impact of Sn–In Codoping on Structural, Morphological, and Optoelectronic Properties of Spray–Deposited ZnO Thin Films

Bijayalaxmi Sahoo <sup>1</sup>, Abinash Pradhan <sup>1</sup>, Shantinarayan Rout <sup>2,\*</sup>, Debadhyan Behera <sup>1,\*</sup>

**ABSTRACT:** This study investigates the influence of Sn–In codoping on the structural, morphological, optical, and photoluminescence properties of ZnO thin films synthesized via spray pyrolysis. The doping concentrations were varied as 1–3 at.% (SIZO1), 3–3 at.% (SIZO3), and 5–3 at.% (SIZO5) for Sn and In, respectively. X-ray diffraction (XRD) analysis revealed a preferential (002) orientation in undoped ZnO, which shifted to (101) in SIZO1 and SIZO3, while SIZO5 exhibited a mixed (002) and (100) orientation. Field-emission scanning electron microscopy (FESEM) showed a transformation from spherical nanoparticles in ZnO to spindle-shaped nanostructures in SIZO1, followed by distorted morphologies in SIZO3 and SIZO5, attributed to lattice strain and increased nucleation sites due to doping. Optical studies demonstrated a reduction in bandgap from 3.28 eV (ZnO) to 3.21 eV (SIZO1), with a slight increase at higher Sn concentrations (3.22–3.23 eV), suggesting bandgap tuning via codoping. Photoluminescence (PL) spectra exhibited near-band-edge emission at 393 nm alongside defect-related transitions at 440–670 nm, associated with intrinsic defects such as zinc vacancies (V<sub>Zn</sub>), oxygen interstitials (O<sub>i</sub>), and zinc interstitials (Zn<sub>i</sub>). The PL intensity quenched in SIZO1 but increased in SIZO3 and SIZO5, indicating dopant-mediated defect engineering. These findings highlight the role of Sn–In codoping in modulating crystallinity, morphology, and optoelectronic properties of ZnO, making it a promising candidate for thin-film optoelectronic applications.

**Keywords:** ZnO thin films, Sn–In codoping, Spray pyrolysis, Optical bandgap tuning, Photoluminescence spectroscopy, Defect-mediated emissions

Received: 05 September 2024; Revised: 29 October 2024; Accepted: 13 January 2025; Published Online: 10 February 2025

## 1. INTRODUCTION

Zinc oxide (ZnO) has emerged as one of the most extensively studied metal oxides due to its exceptional optoelectronic properties, including a wide direct bandgap (~3.37 eV), large exciton binding energy (~60 meV), and high thermal and chemical stability [1,2]. These characteristics make ZnO a promising candidate for a wide range of applications, such as ultraviolet (UV) photodetectors, light-emitting diodes (LEDs), solar cells, gas sensors, and transparent conductive

oxides (TCOs) [3–5]. Additionally, its non-toxicity, abundance, and cost-effectiveness further enhance its industrial viability [6]. However, despite these advantages, the practical utilization of ZnO in electronic devices has been limited by its mediocre electrical conductivity and challenges in achieving precise control over its optical and electronic properties, particularly when synthesized via solution-based techniques [7].

Doping ZnO with selective impurities is a well-established strategy to modulate its electrical and optical properties. Monovalent (Li<sup>+</sup>, Na<sup>+</sup>), divalent (Mg<sup>2+</sup>, Cd<sup>2+</sup>), trivalent (Al<sup>3+</sup>, Ga<sup>3+</sup>, In<sup>3+</sup>), and tetravalent (Sn<sup>4+</sup>, Ti<sup>4+</sup>) dopants have been widely investigated to enhance carrier concentration, reduce resistivity, and tailor the bandgap [8–10]. Among these, indium (In<sup>3+</sup>) doping has been particularly effective due to its higher oxidation state compared to Zn<sup>2+</sup>, despite its larger ionic radius (0.080 nm for In<sup>3+</sup> vs. 0.074 nm for Zn<sup>2+</sup>) [11]. In-doped ZnO (IZO) thin films exhibit

<sup>1</sup> Department of Physics, Ravenshaw University, Cuttack, Odisha-753003, India.

<sup>2</sup> Department of Physics, Amity School of Applied Sciences, Amity University Mumbai, Maharashtra-410206, India.

\*Author to whom correspondence should be addressed:  
[debadhyan\\_25@yahoo.co.in](mailto:debadhyan_25@yahoo.co.in) (Debadhyan Behera)  
[shantinarayan@gmail.com](mailto:shantinarayan@gmail.com) (Shantinarayan Rout)

improved conductivity and optical transparency, making them suitable for transparent electrode applications [12]. Similarly, tin ( $\text{Sn}^{4+}$ ) doping has been explored owing to its smaller ionic radius (0.069 nm), which facilitates substitution at  $\text{Zn}^{2+}$  sites, thereby enhancing n-type conductivity [13]. However, high doping concentrations often lead to solubility limits, carrier scattering, and structural distortions, which degrade electrical performance [14].

To overcome these limitations, codoping—simultaneous incorporation of two or more dopants—has been proposed as an effective approach. Codoping can compensate for lattice strain, improve dopant solubility, and optimize charge carrier concentration by balancing donor and acceptor defects [15]. For instance, Al-Ga, In-Ga, and Al-In codoped ZnO systems have demonstrated superior electrical and optical properties compared to their singly doped counterparts [16–18]. In particular, the Sn-In codoping strategy is of significant interest due to the complementary roles of  $\text{Sn}^{4+}$  (smaller ionic radius, higher charge state) and  $\text{In}^{3+}$  (larger ionic radius, trivalent state) in modifying ZnO's electronic structure. Theoretical and experimental studies suggest that Sn-In codoping can enhance carrier mobility by reducing ionized impurity scattering while maintaining high optical transparency [19, 20].

Several deposition techniques have been employed to fabricate doped ZnO thin films, including sputtering, pulsed laser deposition (PLD), molecular beam epitaxy (MBE), and chemical vapor deposition (CVD) [21, 22]. However, these methods often require high vacuum conditions, sophisticated instrumentation, and elevated costs, limiting their scalability. In contrast, chemical solution deposition techniques, such as sol-gel and spray pyrolysis, offer a low-cost, scalable, and facile route for thin-film synthesis [23]. Spray pyrolysis, in particular, allows for precise stoichiometric control, uniform film deposition, and compatibility with large-area substrates [24]. The properties of spray-deposited ZnO films are highly influenced by precursor chemistry, solvent selection, and doping concentration. For example, methanol-water mixtures have been reported to enhance film morphology and crystallinity compared to aqueous solutions, as they facilitate better precursor dissociation and reduced surface tension during droplet formation [25].

Despite the growing interest in codoped ZnO systems, studies on Sn-In codoped ZnO (SIZO) thin films remain limited. Liu et al. [26] fabricated amorphous In-Sn-Zn-O (a-ITZO) thin-film transistors (TFTs) via ultrasonic spray pyrolysis, achieving high field-effect mobility ( $43.84 \text{ cm}^2\text{V}^{-1}\text{s}^{-1}$ ) and excellent on/off current ratios ( $2.26 \times 10^8$ ). Similarly, Park et al. [27] reported that crystalline ITZO (c-ITZO) TFTs exhibited superior electron mobility and device stability compared to their amorphous counterparts. Sun et al. [28] employed high-power impulse magnetron sputtering to deposit ITZO films, observing that crystallinity and carrier mobility improved with increasing pulse-off time, reaching a resistivity of  $4.07 \times 10^{-3} \Omega\cdot\text{cm}$  and a carrier concentration of  $1.25 \times 10^{20} \text{ cm}^{-3}$ . Su et al. [29] further enhanced the performance of In-Zn-Sn-O (IZTO) TFTs by nitrogen doping, achieving a saturation mobility of  $35.1 \text{ cm}^2\text{V}^{-1}\text{s}^{-1}$  and a

threshold voltage of 0.4 V. Tiwari et al. [30] investigated sol-gel-derived Sn-In codoped ZnO films, observing a reduction in bandgap and optimized optoelectronic properties at a 1:3 at.% Sn-In ratio.

In our previous work on Fe-In codoped ZnO thin films [31], we demonstrated that the choice of solvent (methanol-water vs. pure water) significantly influences film morphology and defect-related photoluminescence. Building on these findings, the present study explores the structural, morphological, optical, and photoluminescence properties of spray-deposited Sn-In codoped ZnO thin films, with a focus on the interplay between doping concentration and defect engineering. We systematically vary the Sn doping level (1–5 at.%) while maintaining a fixed In concentration (3 at.%) to elucidate the effects of codoping on crystallographic orientation, nanoparticle morphology, bandgap modulation, and defect-mediated luminescence.

The novelty of this work lies in its comprehensive investigation of Sn-In codoping effects using a simple, scalable spray pyrolysis technique, with particular emphasis on defect-related optical transitions. By correlating XRD, FESEM, UV-Vis, and PL results, we provide insights into how Sn-In codoping modifies the microstructure and optoelectronic behavior of ZnO. The findings are expected to contribute to the rational design of codoped ZnO thin films for optoelectronic and transparent conductive applications, bridging the gap between fundamental research and industrial implementation.

## 2. EXPERIMENTAL DETAILS

The Sn-In codoped ZnO (SIZO) thin films were deposited on chemically cleaned glass substrates using a spray pyrolysis technique. A 0.1 M precursor solution was prepared by dissolving zinc acetate dihydrate [ $\text{Zn}(\text{CH}_3\text{COO})_2 \cdot 2\text{H}_2\text{O}$ ] in a methanol-deionized water mixture (3:1 volume ratio). For codoped samples, indium trichloride ( $\text{InCl}_3$ ) and stannous chloride dihydrate ( $\text{SnCl}_2 \cdot 2\text{H}_2\text{O}$ ) were added to the precursor solution to achieve Sn-In doping concentrations of 1-3 at.% (SIZO1), 3-3 at.% (SIZO3), and 5-3 at.% (SIZO5), respectively. The solution was sprayed onto substrates heated to 350 °C using compressed dry air as the carrier gas. Post-deposition, all films were annealed at 500 °C for 2 hours in a muffle furnace to improve crystallinity.

The structural properties were analyzed using X-ray diffraction (XRD, Rigaku ULTIMA IV) with Cu-K $\alpha$  radiation ( $\lambda = 1.5406 \text{ \AA}$ ). Surface morphology and elemental composition were examined via field-emission scanning electron microscopy (FESEM, Zeiss Supra 55) coupled with energy-dispersive X-ray spectroscopy (EDX, Oxford Instruments). Optical transmittance spectra (300–800 nm) were recorded using a UV-Vis spectrophotometer (Systronics), and the optical bandgap was determined using Tauc's plot method. Photoluminescence (PL) spectra were acquired at room temperature using a fluorescence spectrophotometer (Edinburgh FLS-980) with a 350 nm

excitation wavelength. Film thickness was measured gravimetrically, and the absorption coefficient ( $\alpha$ ) was calculated from transmittance data. All characterizations were performed at ambient conditions to ensure consistency

### 3. RESULTS AND DISCUSSION

X-ray powder diffraction (XRD) is a rapid, basic nondestructive analytical technique essentially used for phase identification of a finely ground, homogenized materials those are wholly, or partially crystalline in nature. It can provide information on unit cell dimensions. The XRD patterns of all thin film samples are represented in Figure 1. The peaks in the patterns are assigned to the Miller indices according to ICDD JCPDS card No. 36-1451 that corresponds to zincite phase. In case of ZnO film, X-rays are diffracted along two principal directions i.e. (002) and (101). High intensity along (002) direction compared to (101) indicates that most of the crystallites are oriented along c-axis. However, in codoped samples, the crystallites get oriented also along other directions. In other words, codoping favors more the polycrystalline nature of ZnO. All the peaks in the diffraction patterns indicate that  $\text{Sn}^{4+}$  ions are incorporated into ZnO either at  $\text{Zn}^{2+}$  sites or interstitial sites without altering the parent crystal structure.

At low codoping concentrations i.e. in SIZO1 and SIZO3, most intense peak becomes (101) along with appearance of other peaks like (100), (102), (110), (103) and (112) in the diffraction patterns. In SIZO5, the peak along (002) acquires the most intensity; however, increase of intensity for other peaks is also noticeable. Various structural parameters like texture coefficient, crystallite size, lattice spacing, lattice constants, dislocation density and lattice strain are calculated using equations mentioned elsewhere [21, 22]. These values are provided in Table 1.

Looking at the texture co-efficient, ZnO is said to be preferentially oriented along (002) plane as  $\text{TC} > 1$  indicates preferential orientation, otherwise random orientation. When Sn doping level increases, TC for (002) decreases and most crystallites get oriented along (101) in SIZO1 and SIZO3. However, in SIZO5 sample, again (002) orientation is favored most and also (100) orientation to some extent at the cost of (101) orientation. This change in particle orientations is attributed to the induced stress as a result of difference in ionic radii of Zn and Sn [23]. Others attribute it to the decrease in mobility of Zn and O atoms with more presence of Sn atoms [24]. The mechanism of favoring particle growth along a particular plane i.e. (002) in this case suggests minimization of surface free energy along that plane. It is also supported by the fact that crystallite size decreases with higher Sn doping concentration. This may occur due to the increase in nucleation sites at the time of growth of the film and also may occur due to increase in lattice defects as a result of the size difference between  $\text{Sn}^{4+}$  and  $\text{Zn}^{2+}$  ions [25, 26].

The calculated interplanar spacing for different set of

planes are slightly larger than bulk ZnO (JCPDS 36-1451) and it is expected as the crystallites in thin films are stressed. Further, the interplanar spacing decrease with increase in Sn doping concentration. Since the radius of  $\text{Sn}^{4+}$  ion is smaller than that of  $\text{Zn}^{2+}$  ion, it may be assumed  $\text{Sn}^{4+}$  ion replaces  $\text{Zn}^{2+}$  ion easily leading to decrease in interplanar spacing. It is also observed that the lattice parameters decrease with Sn concentration in the codoped samples. Dislocation density and lattice strain increase when Sn doping concentration increases. The obtained high strain is in line of expectation in spray pyrolytic thin films. It is related to formation of point defects (vacancies and site disorders), dislocations, and extended defects [20]. From these observations, it is understood that the difference in the oxidation state and ionic radii of the dopants ( $\text{In}^{3+}$ ,  $\text{Sn}^{4+}$ ) and the host ( $\text{Zn}^{2+}$ ) atoms as well as the doping efficacy has induced such variations in the unit cell parameters.

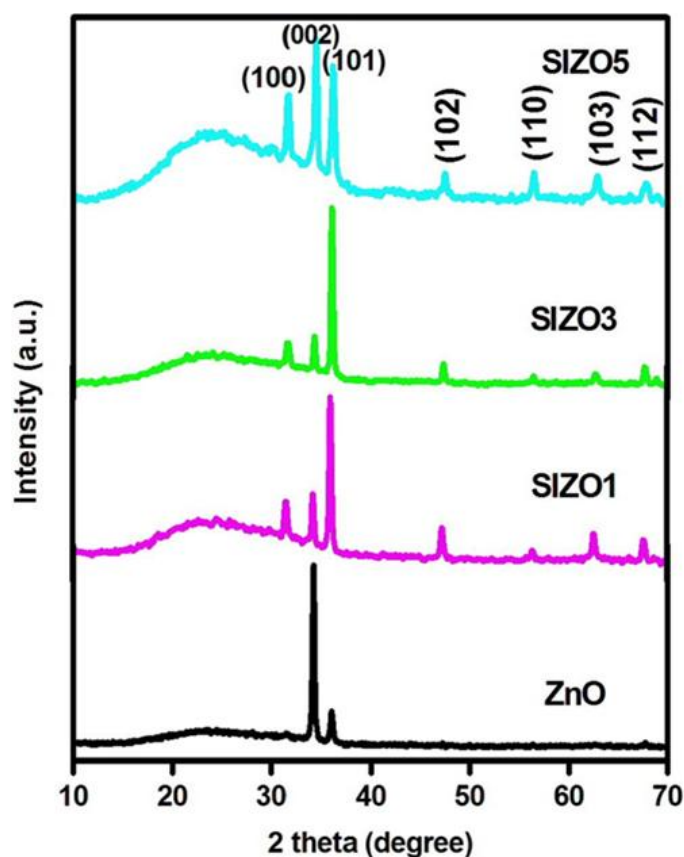


**Fig. 1.** X-ray diffraction patterns of ZnO, SIZO1, SIZO3 and SIZO5 thin films.

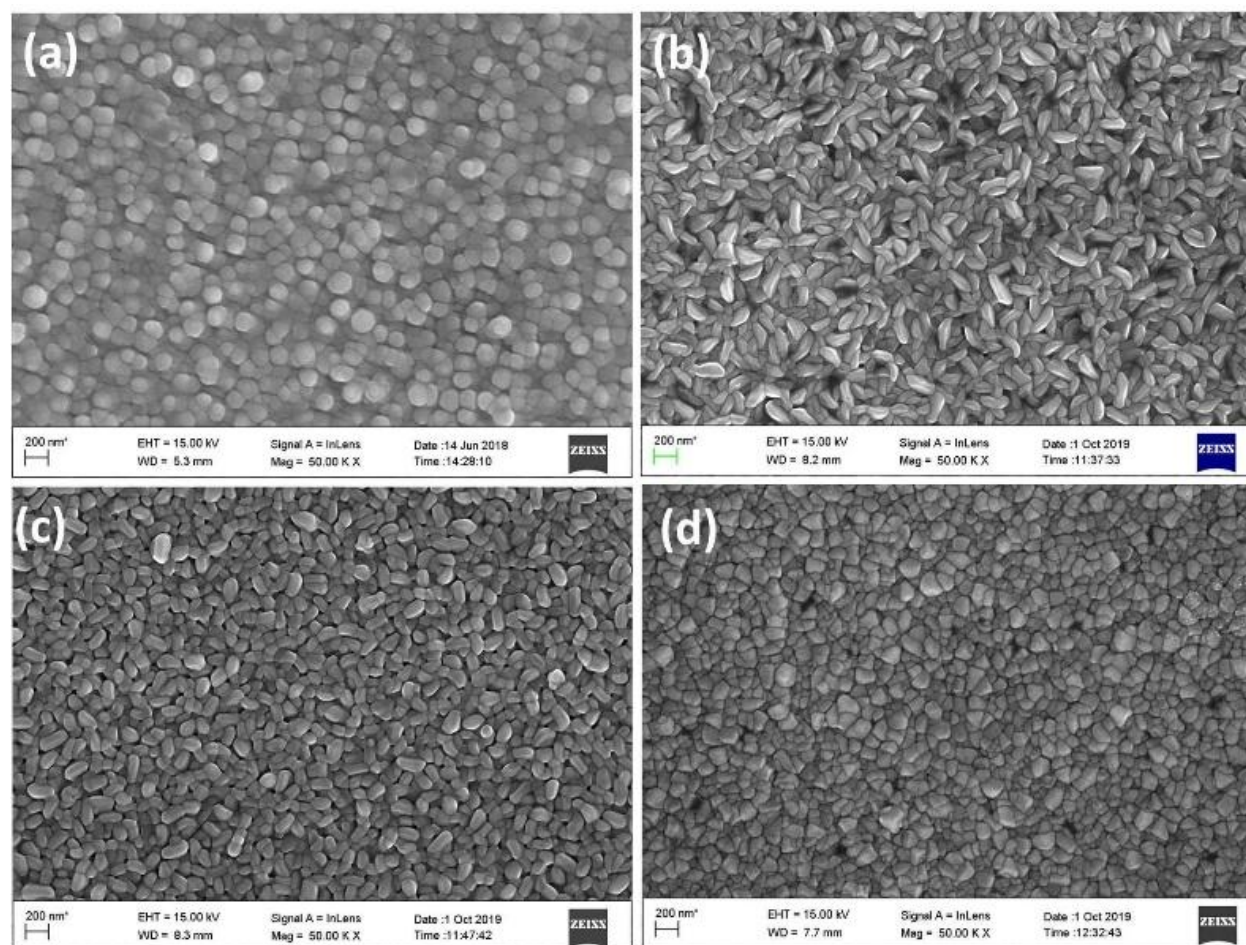
The surface morphology of thin films was probed by FESEM and EDXA. It may be noticed that the surface morphology of thin films undergoes a change with doping. Nanoparticles with spherical morphology are uniformly distributed in ZnO thin film as shown in Figure 2(a). The shape of the nanoparticles changes to that of spindles in SIZO1 as shown in Figure 2(b). Presence of voids may be also noticed on the surface.

**Table 1.** Structural parameters of ZnO, SIZO1, SIZO3 and SIZO5 thin films.

Sample name	Miller indices ( <i>hkl</i> )	Texture coefficient ( <i>TC</i> )	Crystallite size ( <i>D</i> ) nm	Lattice spacing ( <i>d</i> ) Å	Lattice Parameters		Dislocation Density ( $\delta$ ) $\times 10^{10}$ cm <sup>-2</sup>	Strain ( $\sigma$ ) $\times 10^{-3}$
					<i>c</i> (Å)	<i>a</i> (Å)		
<b>ZnO</b>	(002)	1.85	35.8	2.620	5.241	3.270	7.79	3.29
	(101)	0.15	28.7	2.491				
<b>SIZO1</b>	(100)	0.58	28.8	2.834	5.235	3.267	12.08	4.43
	(002)	1.03	32.9	2.617				
	(101)	1.39	31.3	2.492				
<b>SIZO3</b>	(100)	0.43	26.8	2.823	5.222	3.260	13.91	4.74
	(002)	0.82	34.4	2.611				
	(101)	1.73	33.9	2.486				
<b>SIZO5</b>	(100)	0.95	28.2	2.824	5.206	3.261	12.60	4.51
	(002)	1.71	30.1	2.603				
	(101)	0.63	24.7	2.483				

Further increase of Sn doping concentration to 3 at. % (SIZO3) reduces the elongated dimension of nanospindles leading to overall reduction of particle sizes as shown in

Figure 2(c). In SIZO5, the ZnO nanoparticles acquire a completely distorted arbitrary shape with wide size variations and shown in Figure 2(d).

**Fig. 2.** FESEM images of (a) ZnO, (b) SIZO1, (c) SIZO3 and (d) SIZO5 thin films.

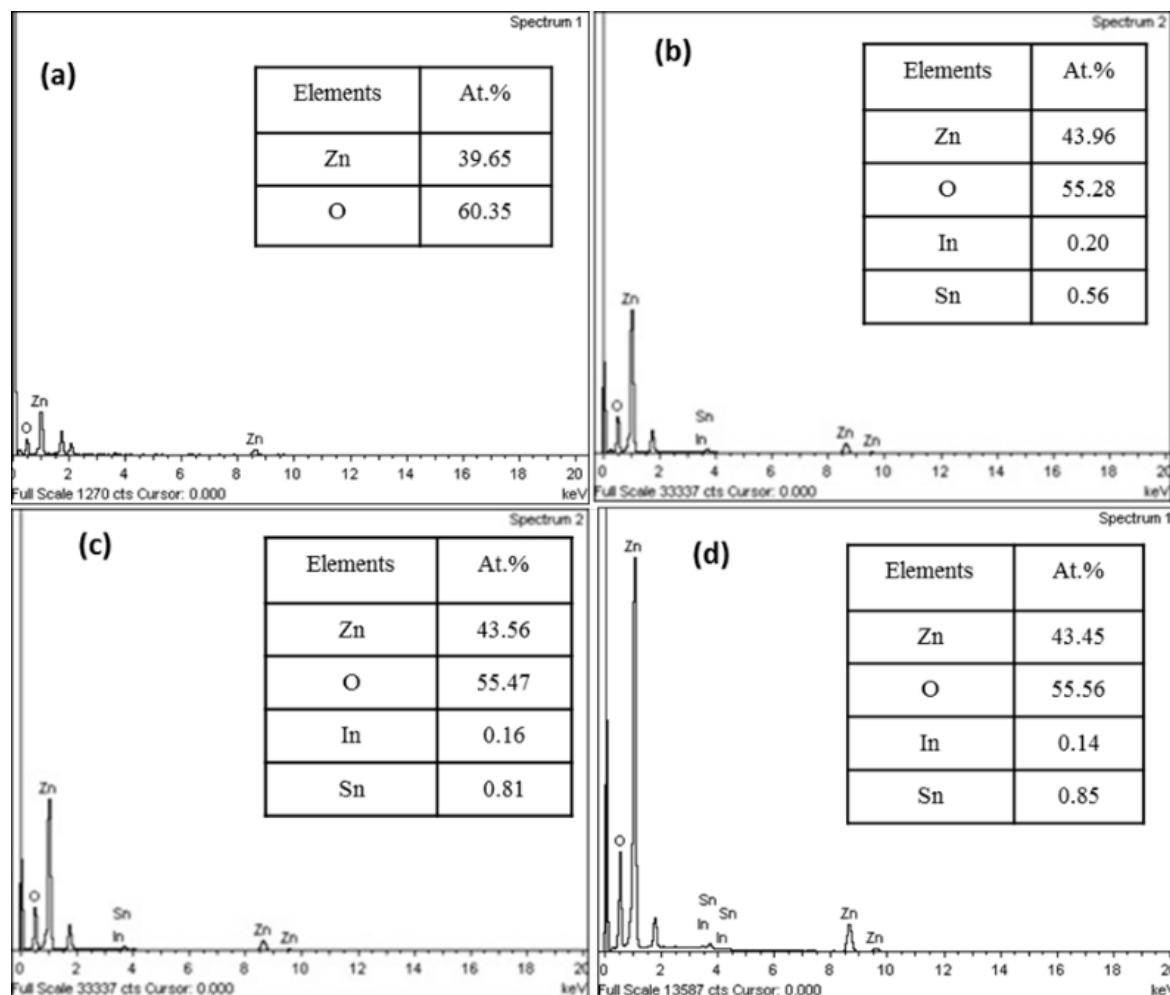


**Fig. 3.** EDXA spectra of (a) ZnO, (b) SIZO1, (c) SIZO3 and (d) SIZO5 thin films.

The elemental distribution in the samples was analyzed by recording EDX spectra. The recorded spectrum for each film and average concentrations (at. %) of constituent elements are shown in Figure 3. It is observed that oxygen concentration is more in comparison to that of zinc in all films. However, this difference in concentration of O and Zn is reduced in codoped samples. The deviation in the concentration of In and Sn in the EDXA data from the actual doping concentration may be due to the semi quantitative nature of the EDX analysis technique.

With increasing Sn doping concentration, particle size decreases which follow a similar variation trend as in crystallite size (measured from XRD patterns). The reduction of particle size may be as a result of availability of a greater number of nucleation sites and the interruption of particle growth by stress due to size difference between  $\text{Zn}^{2+}$  and  $\text{Sn}^{4+}$  ion. By using ImageJ software and by fitting with Gaussian distribution function, the average particle size of each sample was estimated. The mean particle size and full width half maximum for size variation are provided in Figure 4 as inset. It tells that particle size decreases marginally with doping concentration. Due to smaller size of  $\text{Sn}^{4+}$  than  $\text{Zn}^{2+}$  ions, there may be lattice distortions upon substitution. Further, the

$\text{Sn}^{4+}$  ions may act as nucleation sites, and reduce the energy required for particle formation. Thus, increasing Sn doping concentration may lead to smaller particles along with variation of particle morphology.

The optical transmittance spectra of all samples recorded in the wavelength range 300-800 nm are represented in Figure 5. The transmittance at 550 nm decreases from 99% in case of ZnO to 83% in case of SIZO5. This is often attributed to increase of scattering of photons by defects created by doping [23], however, grain boundary scattering may be the reason as there is change in nanoparticle shape and size with doping.

The absorption coefficient ( $\alpha$ ), incident photon energy ( $h\nu$ ) and the optical bandgap ( $E_g$ ) are related with each other by Tauc relation which is written as:

$$(\alpha h\nu)^2 = A(h\nu - E_g) \quad (1)$$

Where  $A$  is the constant.

Thus, the band gap of each film can be known from the intercept made by extrapolated linear portion of  $(\alpha h\nu)^2 \sim h\nu$  plot on  $h\nu$  - axis as depicted in Figure 6.

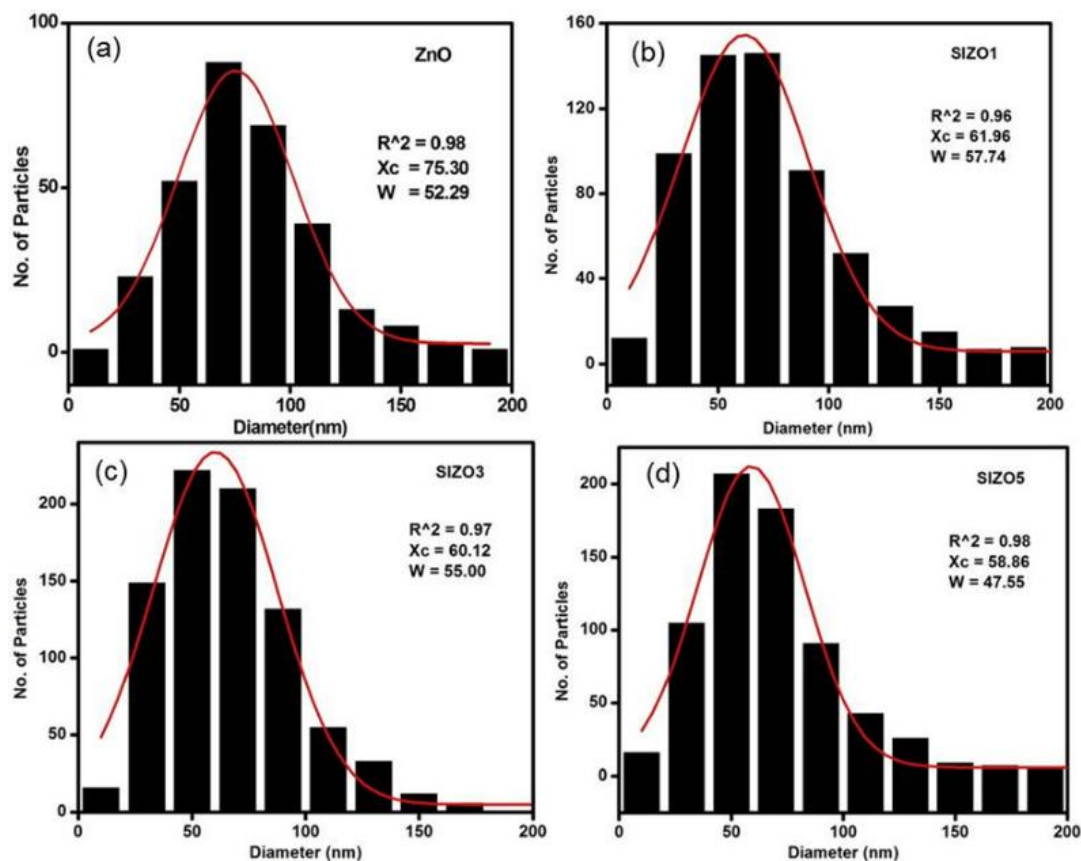


**Fig. 4.** Particle size distribution in (a) ZnO, (b) SIZO1, (c) SIZO3 and (d) SIZO5 thin film.

For this purpose, the absorption coefficient ( $\alpha$ ) was calculated by using Beer-Lambert law [27] given by:

$$\alpha = \frac{\ln(1/T)}{t} \quad (2)$$

Where  $T$  is the transmittance and  $t$  is the thickness of the film. Average thickness ( $t$ ) of each thin film was determined by following gravimetric weight difference method.

Pure ZnO film is found to have band gap of 3.28 eV that decreases to 3.21 eV for SIZO1. The band shrinkage effect may be the reason for decreasing band gap. Sn may be causing development of new type recombination centers possessing lower emission energies [28]. The marginal increase in the band gap for higher doping level (SIZO3 and SIZO5) may be ascribed to the shifting of Fermi level which occurred as a consequence of increasing carrier concentration due to substitution of  $Zn^{2+}$  ions by  $Sn^{4+}$  ions [29].

Photoluminescence emission spectra of all the samples were measured at room temperature in the wavelength range from 370-700 nm by exciting at 350 nm and shown in Figure 7. A strong UV emission peak at 393 nm (3.15 eV) is observed for all the films whose origin is referred to excitonic recombination or near band edge emission (NBE) in ZnO [26]. Besides NBE peak, other emissions at 440 nm (2.82 eV), 450 nm (2.75 eV), 467 nm (2.65 eV), 480 nm (2.58 eV), 490 nm (2.53 eV), 510 nm (2.43 eV), 650 nm (1.91 eV) and 670 nm (1.85 eV) are seen in case of all the films.

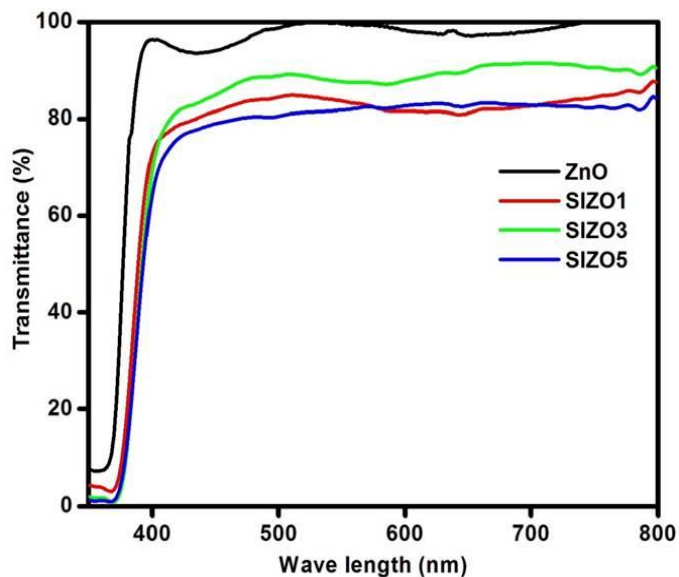


**Fig. 5.** Optical transmission spectra of ZnO, SIZO1, SIZO3 and SIZO5 thin films.

These peaks correspond to electronic transitions associated with different types of intrinsic defects. If the emission intensities in all samples are compared, it may be noticed that though there is no change in peak positions, there is a quenching effect in SIZO1 sample.

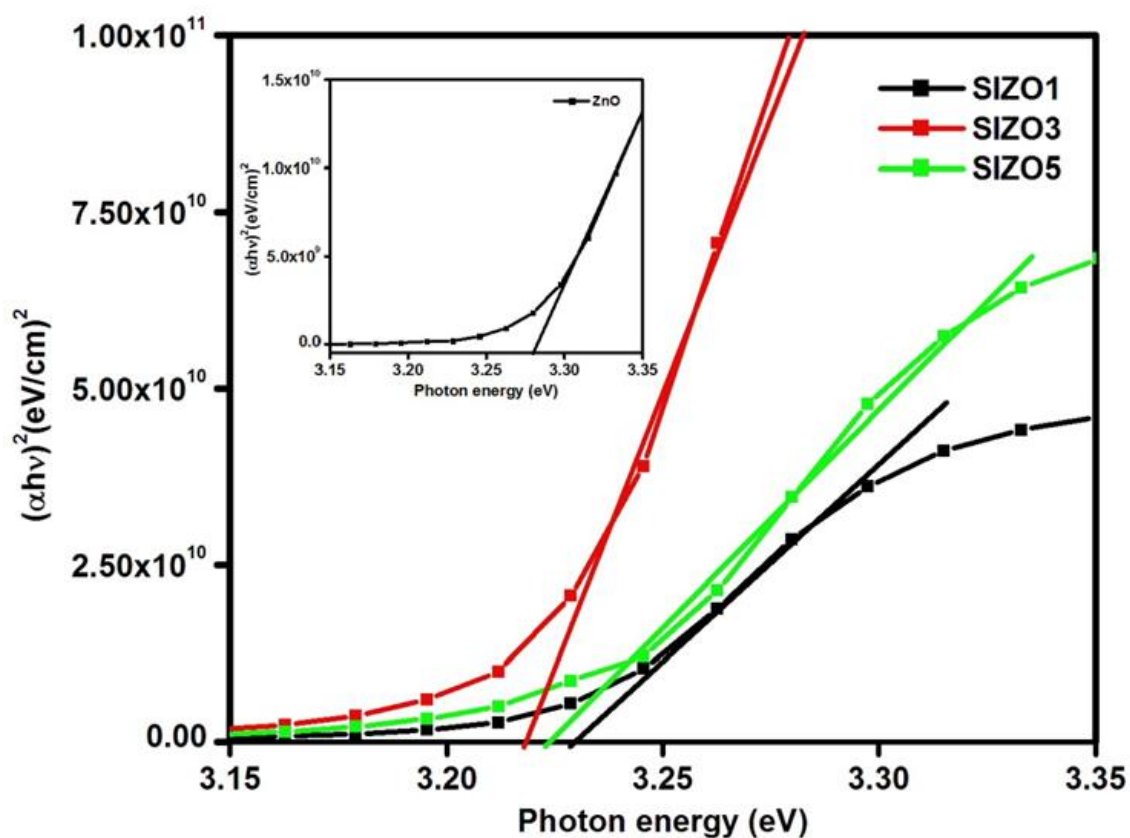


Fig. 6. Tauc's plot for ZnO (Inset), SIZO1, SIZO3 and SIZO5 thin films.

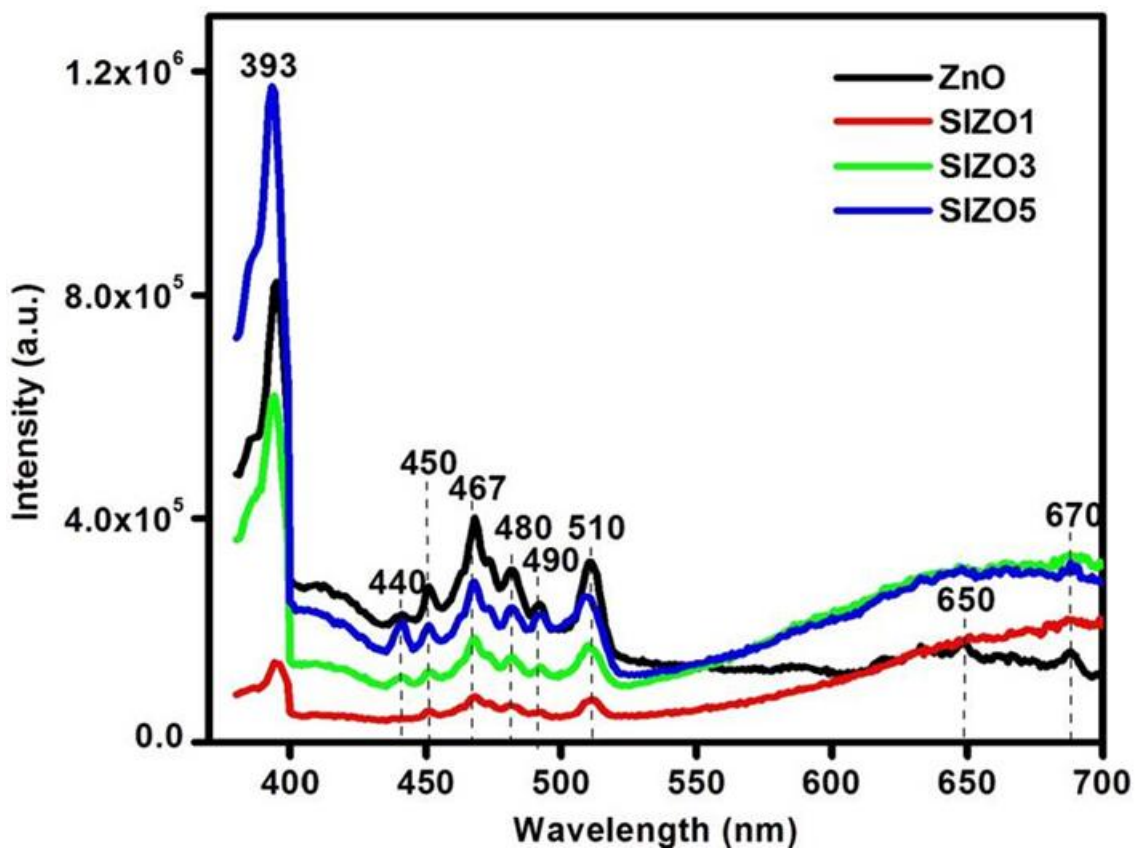


Fig. 7. Photoluminescence emission spectra of ZnO, SIZO1, SIZO3 and SIZO5 thin films (exciting wavelength 350 nm).

**Table 2.** Thickness, Absorption coefficient and Band gap of ZnO, SIZO1, SIZO3 and SIZO5 thin films.

Sample code	Thickness ( $t$ ) in nm	Abs. coefficient ( $\alpha$ ) at $\lambda = 550$ nm	Band gap ( $E_g$ ) in eV
ZnO	650	$2.92 \times 10^{-6}$	3.28
SIZO1	530	$3.35 \times 10^{-4}$	3.21
SIZO3	400	$3.28 \times 10^{-4}$	3.22
SIZO5	480	$3.45 \times 10^{-4}$	3.23

However, in SIZO3 and SIZO5, the emission intensity increases. The decrease in excitonic emission peak is attributed to the non-radiative transition or formation of new recombination centers [30, 31]. However, the quenched emission spectrum in SIZO1 may also be due to less density of intrinsic defects possibly caused by low level of Sn doping.

There are divergent views among researchers about the origin of visible emissions in ZnO. For instance, according to Tiwari et al., the peak at 440 nm is attributed to the zinc interstitials ( $Zn_i$ ) and incorporation of  $Sn^{4+}$  ion into ZnO lattice causes the enhancement of this peak [32]. The peak at 450 nm and 467 nm are associated with zinc vacancies ( $V_{Zn}$ ) and singly ionized oxygen vacancies ( $V_O^+$ ) [33]. The peak at 480 nm originates due to electronic transition from a shallow donor state ( $Zn_i$ ) to a deep acceptor state ( $V_{Zn}$ ). The emissions at 490 nm and 510 nm are related to oxygen vacancies [34]. When a photogenerated hole recombines with electron of the singly ionized oxygen ( $V_O$ ) vacancies in the surface lattices of the ZnO, deep level emission (DPE) occurred which may be related to the green emission [29]. The radiative transitions between shallow donors (related to  $V_O$ ) and deep acceptors ( $V_{Zn}$ ) may be also related to the green emission [35]. The red emission peak at 650 nm and far-red emission peak at 670 nm have been assigned to zinc interstitial ( $Zn_i$ ), zinc/tin vacancies ( $V_{Zn}/V_{Sn}$ ), residual strain, crystal defects or Zn/Sn stoichiometry [36]. Table 2 summarizes the thickness, absorption coefficient ( $\alpha$ ), and optical bandgap ( $E_g$ ) of undoped ZnO and Sn-In codoped ZnO (SIZO) thin films. The undoped ZnO film exhibits the highest thickness (650 nm), which decreases to 530 nm for SIZO1 (1 at.% Sn) and further reduces to 400 nm for SIZO3 (3 at.% Sn), before slightly increasing to 480 nm for SIZO5 (5 at.% Sn). This variation in thickness is attributed to changes in nucleation and growth kinetics induced by Sn-In codoping.

The absorption coefficient ( $\alpha$ ) at 550 nm increases significantly from  $2.92 \times 10^{-6}$  (ZnO) to  $3.35 \times 10^{-4}$  (SIZO1), indicating enhanced light absorption due to defect states introduced by doping. While  $\alpha$  remains relatively stable for SIZO3 ( $3.28 \times 10^{-4}$ ) and SIZO5 ( $3.45 \times 10^{-4}$ ), the higher values compared to ZnO suggest persistent defect-mediated absorption. The bandgap of ZnO (3.28 eV) narrows to 3.21 eV for SIZO1, likely due to band-tailing effects from impurity states. However, with increasing Sn concentration (SIZO3 and SIZO5), the bandgap slightly increases to 3.22–3.23 eV, possibly due to the Burstein-Moss effect, where higher carrier concentrations fill conduction band states, leading to an apparent widening of the gap. These trends highlight the tunability in the optical properties of ZnO via

Sn-In codoping.

In our earlier report for Fe-In codoped ZnO thin films [21], similar peaks at 393 nm, 450 nm, 467 nm, 480 nm, 510 nm are obtained as in case of SIZO thin films. An additional peak at 415 nm is seen that may correspond to transitions of electrons from conduction band to zinc vacancies. Following these attributions, it looks inconclusive as samples are deposited in O-rich conditions while decrease of oxygen vacancies also leads to increase of Zn vacancies. However, it is certain that the defects like interstitials and vacancies are the major contributors by some means to the luminescence properties of ZnO. The extrinsic dopants only influences the density of these various defects, thereby the nature of the photoluminescence spectrum in each sample. In this scenario, if the energy levels of various intrinsic defects in ZnO based on different theoretical calculations [37, 38] and the proposed transition mechanism [39] are considered by assuming that there is slight deviation in the energy of the intrinsic defects within limit, then the visible emissions observed in these samples may be related to the electronic transitions as 440 nm (from exciton level to  $V_{Zn}$ ), 450 nm (from exciton level to  $O_i$ ), 467 nm/480 nm (from  $Zn_i$  to  $V_{Zn}$ ), 490 nm/510 nm (from  $Zn_i$  to  $O_i$ ), 650 nm (from  $Zn_i$  to  $O_{Zn}$  or from  $V_OZn_i$  to  $V_{Zn}$ ) and 670 nm (conduction band to  $O_{Zn}$ ).

## 4. CONCLUSION

This study systematically explored the effects of Sn-In codoping on the microstructure, morphology, optical absorption, and photoluminescence properties of ZnO thin films deposited via spray pyrolysis. XRD analysis confirmed the hexagonal wurtzite structure of ZnO, with codoping inducing a shift in preferential crystallographic orientation from (002) in undoped ZnO to (101) in SIZO1 and SIZO3, followed by a partial reversion to (002) in SIZO5. This transition is attributed to lattice strain and altered growth kinetics due to the incorporation of  $Sn^{4+}$  and  $In^{3+}$  ions. FESEM revealed a progressive evolution in nanoparticle morphology—from spherical (ZnO) to spindle-shaped (SIZO1) and finally to irregular nanostructures (SIZO3 and SIZO5)—indicating that higher Sn concentrations disrupt particle growth uniformity, likely due to increased nucleation sites and lattice distortion. Optical studies demonstrated bandgap narrowing from 3.28 eV (ZnO) to 3.21 eV (SIZO1), suggesting band-tailing effects induced by defect states. The marginal increase in bandgap for SIZO3 and SIZO5 may

arise from Burstein-Moss shift due to enhanced carrier concentration. Photoluminescence spectra exhibited a dominant near-band-edge emission at 393 nm, alongside defect-related emissions (440–670 nm) linked to transitions involving zinc vacancies (VZn), oxygen interstitials (Oi), and zinc interstitials (Zni). The PL quenching in SIZO1 implies suppressed non-radiative recombination, while intensified emissions in SIZO3 and SIZO5 suggest increased defect density at higher Sn concentrations. The findings underscore the efficacy of Sn-In codoping in tailoring the structural and optoelectronic properties of ZnO. The tunable bandgap and defect-mediated luminescence highlight potential applications in UV photodetectors, light-emitting diodes, and transparent conductive oxides. Future work should focus on optimizing doping ratios to enhance electrical conductivity while minimizing defect-induced scattering, thereby advancing the utility of codoped ZnO in next-generation optoelectronic devices.

## DECLARATIONS

### Ethical Approval

We affirm that this manuscript is an original work, has not been previously published, and is not currently under consideration for publication in any other journal or conference proceedings. All authors have reviewed and approved the manuscript, and the order of authorship has been mutually agreed upon.

### Funding

Not applicable

### Availability of data and material

All of the data obtained or analyzed during this study is included in the report that was submitted.

### Conflicts of Interest

The authors declare that they have no financial or personal interests that could have influenced the research and findings presented in this paper. The authors alone are responsible for the content and writing of this article.

### Authors' contributions

All authors contributed equally in the preparation of this manuscript.

## ACKNOWLEDGEMENTS

The authors gratefully acknowledge the financial assistance received from ANRF, New Delhi, Govt. of India (Project File No. SUR/2022/001738) and the help extended by Department of Geology, Ravenshaw University, Cuttack for XRD analytical facility.

## REFERENCE

- [1] Özgür, Ü., Alivov, Y.I. and Liu, C., et al. **2005**. A comprehensive review of ZnO materials and devices. *Journal of Applied Physics*, 98, pp.1-103.
- [2] Kołodziejczak-Radzimska, A. and Jesionowski, T., **2014**. Zinc Oxide—From Synthesis to Application: A Review. *Materials (Basel)*, 7, pp.2833-2881.
- [3] Bhosale, S.R., Bhosale, R.R., Patil, V.L., Dhavale, R.P., Shukla, S.S., Gadale, S.R. and Anbhule, P.V., **2024**. Superior antibacterial performance of surfactant-assisted ZnO nanoflakes produced via Co-precipitation method. *Chemical Physics Letters*, 846, pp.141318.
- [4] Bhosale, S.R., Bhosale, R.R., Moyo, A.A., Shinde, S.B., Yadav, T.B., Dhavale, R.P., Chalapathi, U., Patil, D.R. and Anbhule, P.V., **2023**. Effect of Zn doping on antibacterial efficacy of CuO nanostructures. *ChemistrySelect*, 8(34), p. e202301997.
- [5] Pavithra T., Althaf M., and Ganesh L., et al. **2025**. Synthesis of Zinc-Doped Iron Oxide nanomaterials using *Cissus quadrangularis*: characterizations and Photocatalytic applications. *SciEngg Advances*, 2, pp. 35-43.
- [6] Ganie, A.S., Hussain, S., Shah, S., Liaqat, M.J., Begi, A.N., Miao, Z. and Han, Y., **2024**. In<sub>2</sub>O<sub>3</sub> doped ZnO nanosheets for ultra-trace detection of NO<sub>2</sub>. *SciEngg Advances*, 1(2), pp.56-65.
- [7] Janotti, A. and Van De Walle, C.G., **2009**. Fundamentals of zinc oxide as a semiconductor. *Reports on Progress in Physics*, 72, pp.126501.
- [8] Pearton, S.J., Norton, D.P. and Ip, K., et al. **2005**. Recent progress in processing and properties of ZnO. *Progress in Materials Science*, 50, pp.293-340.
- [9] Paraguay, D. F., Morales, J. and Estrada, L. W., et al. **2000**. Influence of Al, In, Cu, Fe and Sn dopants in the microstructure of zinc oxide thin films obtained by spray pyrolysis. *Thin Solid Films*, 366, pp.16-27.
- [10] Bedia, F.Z., Bedia, A. and Maloufi, N., et al. **2014**. Effect of tin doping on optical properties of nanostructured ZnO thin films grown by spray pyrolysis

- technique. *Journal of Alloys and Compounds*, 616, pp.312-318.
- [11] Ilican, S., Caglar, M. and Caglar, Y., **2010**. Sn doping effects on the electro-optical properties of sol gel derived transparent ZnO films. *Applied Surface Sciences*, 256, pp.7204-7210.
- [12] Alsaad, A.M., Ahmad, A.A., Qattan, I.A., Al-Bataineh, Q.M. and Albatineh, Z., **2020**. Structural, optoelectrical, linear, and nonlinear optical characterizations of dip-synthesized undoped ZnO and group III elements (B, Al, Ga, and In)-doped ZnO thin films. *Crystals*, 10, pp.252.
- [13] Pal, S., Ghosh, S. and Basak, D., **2021**. Room temperature deposition of pulsed laser-assisted (Al, In) co-doped ZnO transparent conducting films appropriate for flexible substrates. *Journal of Materials Science: Materials in Electronics*, 32, pp.16682-16693.
- [14] Koksai, N.E., Sbeta, M., Atilgan, A. and Yildiz, A., **2021**. Al-Ga co-doped ZnO/Si heterojunction diodes. *Physica. B: Condensed Matter*, 600, pp.412599.
- [15] Li, F., Meng, Y., Kang, X., Yip, S., Bu, X., Zhang, H. and Ho, J.C., **2020**. High-mobility In and Ga co-doped ZnO nanowires for high-performance transistors and ultraviolet photodetectors. *Nanoscale*, 12, pp.16153-16161.
- [16] Liu, H. Y., Hsu, W. C., Chen, J. H., Hsu, P. H. and Lee, C. S., **2020**. Amorphous ITZO Thin-Film Transistors by Using Ultrasonic Spray Pyrolysis Deposition. *IEEE Transactions on Electron Devices*, 67, pp.1009-1013.
- [17] Park, S., Park, K., Kim, H., Park, H.W., Chung, K.B. and Kwon, J.Y., **2020**. Light-induced bias stability of crystalline indium-tin-zinc-oxide thin film transistors. *Applied Surface Science*, 526, pp.146655.
- [18] Sun, H., Li, Z.Y., Chen, S.C., Liao, M.H., Gong, J.H., Bai, Z. and Wang, W.X., **2021**. In-Sn-Zn Oxide Nanocomposite Films with Enhanced Electrical Properties Deposited by High-Power Impulse Magnetron Sputtering. *Nanomaterials*, 11, pp.2016.
- [19] Su, J., Wang, Y., Ma, Y., Wang, Q., Tian, L., Dai, S., Li, R., Zhang, X. and Wang, Y., **2018**. Preparation and electrical characteristics of N-doped In-Zn-Sn-O thin film transistors by radio frequency magnetron sputtering. *Journal of Alloys and Compounds*, 750, pp.1003-1006.
- [20] Tiwari, A. and Sahay, P.P., **2020**. The effects of Sn-In co-doping on the structural, optical, photoluminescence and electrical characteristics of the sol-gel processed ZnO thin films. *Optical Materials*, 110, pp.110395.
- [21] Sahoo, B., Pradhan, S.K., Mishra, D.K., Sahoo, S.K., Nayak, R.R. and Behera, D., **2021**. Mutual effect of solvent and Fe-In codoping on structural, optical and electronic properties of ZnO thin films prepared by spray pyrolysis technique. *Optik*, 228, pp.166134.
- [22] Cullity, B.D., **1956**. *Elements of X-ray Diffraction*, Addison-Wesley Publishing.
- [23] Acharya, A.D., Moghe, S. and Panda, R., et al. **2012**. Growth and characterization of nano-structured Sn doped ZnO. *Journal of Molecular Structure*, 1022, pp.8-15.
- [24] Dhamodharan, P., Manoharan, C. and Dhanapandian, S., et al. **2015**. Preparation and characterization of spray deposited Sn-doped ZnO thin films onto ITO substrates as photoanode in dye sensitized solar cell. **2015**. *Journal of Materials Science: Materials in Electronics*, 26, pp.4830-4839.
- [25] Prajapati, C.S., Kushwaha, A. and Sahay, P.P., **2013**. Optoelectronics and formaldehyde sensing properties of tin-doped ZnO thin films. *Applied Physics A: Materials Science and Processing*, 113, pp.651-662.
- [26] Bindu, P. and Thomas, S., **2014**. Estimation of lattice strain in ZnO nanoparticles: X-ray peak profile analysis. *Journal of Theoretical and Applied Physics*, 8, pp.123-134.
- [27] Pankove, J.I., **1975**. *Optical processes in semiconductors*. Courier Corporation.
- [28] Ilican, S., Caglar, M. and Caglar, Y., **2010**. Sn doping effects on the electro-optical properties of sol gel derived transparent ZnO films. *Applied Surface Science*, 256, pp.7204-7210.
- [29] Agarwal, M.B., Sharma, A., Malaidurai, M. and Thangavel, R., **2018**. Effect of Sn doping on structural, mechanical, optical and electrical properties of ZnO nanoarrays prepared by sol-gel and hydrothermal process. *Superlattices Microstruct*, 117, pp.342-350.
- [30] Look, D.C., Hemsky, J. W. and Sizelove, J. R., **1999**. Residual native shallow donor in ZnO. *Physical Review Letters*, 82, pp.2552-2555.
- [31] Kumar, A. S., Huang, N. M. and Nagaraja, H. S., **2014**. Influence of Sn doping on photoluminescence and photoelectrochemical properties of ZnO nanorod arrays. *Electronic Materials Letters*, 10, pp.753-758.
- [32] Tiwari, A. and Sahay, P. P., **2020**. Sn-Ga co-doping in sol-gel derived ZnO thin films: Studies of their microstructural, optical, luminescence and electrical properties. *Materials Science in Semiconductor Processing*, 118, pp.105178.

- [33] Ravichandran, K., Vasanthi, M., Thirumurugan, K., Sakthivel, B. and Karthika, K., **2014**. Annealing induced reorientation of crystallites in Sn doped ZnO films. *Optical Materials*, 37, pp.59-64.
- [34] McCluskey, M. D. and Jokela, S. J., **2009**. Defects in ZnO. *Journal of Applied Physics*, 106, pp.071101.
- [35] Umar, A., Ribeiro, C., Al-Hajry, A., Masuda, Y. and Hahn, Y. B., **2009**. Growth of highly c-axis-oriented ZnO nanorods on ZnO/glass substrate: Growth mechanism, structural, and optical properties. *Journal of Physical Chemistry C*, 113, pp.14715-14720.
- [36] Lin, H. F., Liao, S. C., Hung, S. W. and Hu, C. T., **2009**. Thermal plasma synthesis and optical properties of Zn<sub>2</sub>SnO<sub>4</sub> nanopowders. *Materials Chemistry and Physics*, 117, pp.9-13.
- [37] Zhang, S. B., Wei, S. H. and Zunger, A., **2001**. Intrinsic n-type versus p-type doping asymmetry and the defect physics of ZnO. *Physical Review B: Condensed Matter and Materials*. 63, pp. 075205.
- [38] Egelhaaf, H. J. and Oelkrug, D., **1996**. Luminescence and nonradiative deactivation of excited states involving oxygen defect centers in polycrystalline ZnO. *Journal of Crystal Growth*, 161, pp.190-194.
- [39] Behera, D. and Acharya, B.S., **2008**. Nano-star formation in Al-doped ZnO thin film deposited by dip-dry method and its characterization using atomic force microscopy, electron probe microscopy, photoluminescence and laser Raman spectroscopy. *Journal of Luminescence*, 128, pp.1577-1586.